Prenatal Bisphenol A Exposure in Mice Induces Multi-tissue Multi-omics Disruptions Linking to Cardiometabolic Disorders

Le Shu[1,2¶], Qingying Meng[1¶], Brandon Tsai[1], Graciel Diamente[1], Yen-wei Chen[3], Andrew Mikhail[1], Helen Luk[1], Beate Ritz[4,5], Patrick Allard[5], and Xia Yang[1,2,3,6*]

[1]Department of Integrative Biology and Physiology, University of California, Los Angeles, CA 90095, USA

[2]Molecular, Cellular, and Integrative Physiology Interdepartmental Program, University of California, Los Angeles, CA 90095, USA

[3]Molecular Toxicology Interdepartmental Program, University of California, Los Angeles, CA 90095, USA

[4]Department of Epidemiology, Fielding School of Public Health, University of California, Los Angeles, CA 90095, USA

[5]Department of Environmental Health Sciences, Fielding School of Public Health, University of California, Los Angeles, CA 90095, USA

[6]Institute for Quantitative and Computational Biosciences, University of California, Los Angeles, CA 90095, USA

[*]**Corresponding author:**

Email: xyang123@ucla.edu (XY)

[¶]**These authors contributed equally to this work**

Abstract

The health impacts of endocrine disrupting chemicals (EDCs) remain debated and their tissue and molecular targets are poorly understood. Here we leveraged systems biology approaches to assess the target tissues, molecular pathways, and gene regulatory networks associated with prenatal exposure to the model EDC Bisphenol A (BPA). Prenatal BPA exposure led to scores of transcriptomic and methylomic alterations in the adipose, hypothalamus, and liver tissues in mouse offspring, with cross-tissue perturbations in lipid metabolism as well as tissue-specific alterations in histone subunits, glucose metabolism and extracellular matrix. Network modeling prioritized main molecular targets of BPA, including *Pparg*, *Hnf4a*, *Esr1*, and *Fasn*. Lastly, integrative analyses identified the association of BPA molecular signatures with cardiometabolic phenotypes in mouse and human. Our multi-tissue, multi-omics investigation provides strong evidence that BPA perturbs diverse molecular networks in central and peripheral tissues, and offers insights into the molecular targets that link BPA to human cardiometabolic disorders.

Author summary

The inability to pinpoint the mechanistic underpinnings of environmentally-induced diseases likely stems from the pleiotropic effects of chemicals such as BPA on diverse tissues and molecular space (transcriptome, epigenome, etc.). This makes it challenging to fully dissect their health impact and merits a call for modern big data approaches to examine environmental factors. Our data-driven study is the first unbiased, multi-tissue multi-omic systems biology investigation of the molecular circuitry and mechanisms underlying offspring response to prenatal BPA exposure. Importantly, the incorporation of network-based modeling allows us to capture novel players in the regulation of BPA activities *in vivo*, and the integration with human disease association datasets

helps bridge the molecular pathways affected by BPA with diverse human diseases. In doing so, our study provides compelling molecular evidence that developmental BPA exposure significantly perturbs metabolic and endocrine systems in the offspring, and supports BPA as one of the environmental factors involved in the developmental origins of health and disease (DOHaD).

Introduction

A central concept in the Developmental Origins of Health and Disease (DOHaD) states that adverse environmental exposure during early developmental stages is an important determinant for later onset adverse health outcomes, even in the absence of continuous exposure in adulthood [1-3]. BPA is one of the most influential environmental metabolic disruptors identified to date with widespread exposure in human populations and likely plays a role in DOHaD. BPA is used in the production of synthetic polymers, including epoxy resins and polycarbonates [4]. The advantageous mechanical properties of BPA have resulted in its ubiquitous use in everyday goods such as plastic bottles and inner coating of canned foods [5,6]. BPA exposure has been confirmed in the majority of human populations [7] and has been linked to body weight, obesity, insulin resistance, diabetes, metabolic syndrome (MetS), and cardiovascular diseases in both human epidemiologic and animal studies [8-15]. Importantly, it has been suggested that the developing fetus is particularly vulnerable to BPA exposure [8,16]. Intrauterine growth retardation (IUGR) has been consistently observed after developmental BPA exposure at intake doses below the suggested human safety level and has been associated with low birth weight, elevated adult fat weight and altered glucose homeostasis [8,17-20]. As a result, BPA has been banned from baby products in Europe, Canada, and the US. However, BPA is still in use in non-baby products, posing continuous exposure to adults. Additionally, BPA has been associated with a transgenerational influence on obesity and MetS [21-23], contributing to a lingering effect of BPA exposure on future generations even under usage restriction. Together these lines of evidence support an intriguing hypothesis that BPA may have been playing an important role in the rise of MetS and cardiometabolic diseases worldwide in the past decades [24-26].

Despite numerous findings connecting BPA with adverse health outcomes, there remain ample conflicting data, as summarized by the European Food Safety Agency [27] and the BPA Joint Emerging Science Working Group of the US FDA. Although inconsistencies across studies might be attributable to non-monotonic dose response, exposure window difference, and varying susceptibility between testing models [13,28], there are also several

additional layers of complexity and challenges hindering the full dissection of the biological effects of BPA. First, previous studies examining BPA in various cell types and tissues suggest a broad impact on biological systems [23,29-31]. Second, BPA has been found to modulate multidimensional molecular events, such as gene expression and epigenetic changes, that are functionally important for processes such as metabolism and immune response [32-37]. However, due to most studies being designed to focus on one factor at a time as well as non-comparable study designs, it is difficult to directly compare effects across tissues or types of molecular data to derive the molecular rules of sensitivity to BPA exposures. In a recent National Toxicology Program report, CLARITY-BPA, where multiple organs were examined, evidence of weight gain and cardiac dysfunctions were observed, however, the study was designed to be solely descriptive and no mechanism of action was proposed. These research gaps in our understanding of the pleiotropy of EDCs and toxicant biological actions necessitated the establishment of the NIEHS TaRGET consortium and a more recent call for the research community to systemically interrogate multiple omics in multiple tissues to accelerate the discovery of key biological fingerprints of environmental exposure [38].

Here we present a multi-tissue, multi-omics systems biology study to examine the systems level influence of prenatal BPA exposure using modern integrative genomics and network modeling approaches in a mouse model. We first utilized next-generation sequencing technologies to characterize perturbations in both the transcriptome and the epigenome across three tissues (white adipose tissue, hypothalamus, liver) in mouse offspring who had experienced *in utero* exposure to BPA. Based on mounting evidence that genes operate in highly complex tissue-specific regulatory networks, we hypothesized that prenatal BPA exposure induces genomic and epigenomic reprogramming in the offspring by affecting the organization and function of tissue-specific gene networks [39-42]. Using both transcription factor (TF) networks and Bayesian networks, we modeled the dynamics of transcriptomic and epigenomic signatures and predicted potential regulators that govern the actions of BPA. Furthermore, the transcriptome, epigenome, and network information was layered upon metabolic phenotypes such as body weight, adiposity, circulating lipids, and glucose levels in the mouse offspring to evaluate disease

association. Lastly, to assess the relevance of the BPA molecular targets identified in our mouse model for human diseases, we applied integrative genomics to bridge the mouse molecular signatures and genetic disease association data from human studies. Our study represents a comprehensive data-driven, systems-level investigation of the molecular and health impact of BPA.

Methods

Ethics statement

All animal experiments were performed in accordance with the Institutional Animal Care and Use Committee (IACUC) guidelines. Animal studies and procedures were approved by the Chancellor's Animal Research Committee of the University of California, Los Angeles (Protocol #2012-059-21).

Overall study design

As shown in **Fig 1A**, pregnant C57BL/6 mice were exposed to BPA during gestation via oral gavage at the dosage of 5mg/kg/day, situated below most reported no-observed-adverse-effect-level (NOAEL) according to toxicity testing (https://comptox.epa.gov/dashboard/dsstoxdb/results?search=Bisphenol+A). This dosage was typically used in previous studies [23,43-45], and was chosen as a proof-of-concept for our systems biology study design and to facilitate comparison with previous studies. Male and female offspring (n = 9 for control and n = 11 for BPA in male; n = 9 for control and n = 13 for BPA in female) of weaning age (3-weeks) were examined for a spectrum of metabolic phenotypes (detailed below), and euthanized to collect key metabolic tissues including white adipose tissue, hypothalamus, and liver. We chose the weaning age in order to investigate early molecular and phenotypic changes in the offspring, which may predispose the offspring to late onset diseases. At the molecular level, we conducted RNA sequencing (RNA-seq) to evaluate transcriptomic alterations, and investigated perturbed biological pathways. We also used reduced representation bisulfite sequencing (RRBS) to

uncover the epigenomic impact of prenatal BPA exposure at millions of methylation sites and analyzed the connection of the epigenomic alterations to changes in the transcriptome. We then integrated the transcriptomic and epigenomic signatures with two types of regulatory networks, namely, transcription factor networks to identify perturbed TF hotspots, and gene regulatory networks to identify non-TF regulatory genes. Finally, we interrogated the associations of the transcriptomic and epigenomic signatures of BPA obtained from our study with metabolic phenotypes in our mouse offspring by correlative analysis, and with human diseases by querying top reported candidate genes as well as full summary statistics from existing publicly available genome-wide association studies (GWAS).

Mouse model of prenatal BPA exposure

Inbred C57BL/6 mice were maintained on a special diet 5V01 (LabDiet), certified to contain less than 150ppm estrogenic isoflavones, and housed under standard housing conditions (room temperature 22–24°C) with 12:12 hr light:dark cycle before mating at 8-10 weeks of age. Upon mating, female mice were randomly assigned to either the BPA treatment group or the control group. From 1-day post-conception (dpc) to 20 dpc, BPA (Sigma-Aldrich, St. Louis, MO) dissolved in corn oil was administered to pregnant female mice via oral gavage (mimicking common exposure route in humans) at 5mg/kg/day on a daily basis. Control mice were fed the same amount of empty vehicle. BPA exposure was restricted to experimental manipulation through the use of polycarbonate-free water bottles and cages. Offspring from each treatment were maintained on a standard chow diet (Newco Distributors Inc, Rancho Cucamonga, CA). Offspring in the vehicle- and BPA-treated groups were derived from 3 and 4 litters by different dams, respectively, to help assess and adjust for litter effects.

Characterization of cardiometabolic phenotypes and tissue collection

Body weight of offspring was measured daily from postnatal day 5 up to the weaning age of 3 weeks. Mice were fasted overnight before sacrifice, and plasma samples were collected through retro-orbital bleeding. Serum lipid and glucose traits including total cholesterol, high density lipoprotein cholesterol (HDL), un-esterified cholesterol

(UC), triglyceride (TG), free fatty acid (FFA), and glucose were measured by enzymatic colorimetric assays at UCLA GTM Mouse Transfer Core as previously described [40]. Gonadal white adipose tissue, hypothalamus, and liver tissues were collected from each animal, flash frozen in liquid nitrogen, and stored at –80°C. For white adipose tissue, we chose the gonadal depot mainly due to its similarity to abdominal fat, established relevance to cardiometabolic risks, tissue abundance, and the fact that it is the most well-studied adipose tissue in mouse models. All mouse experiments were conducted in accordance with and approved by the Institutional Animal Care and Use Committee at University of California, Los Angeles.

RNA sequencing (RNA-seq) and data analysis

A total of 18 RNA samples were isolated from gonadal adipose, hypothalamus and liver tissues (n = 3 per group per tissue; for each group, mice were randomly selected from litters of different dams in independent cages) from male offspring using the AllPrep DNA/RNA Mini Kit (QIAGEN GmbH, Hilden, Germany). We focused on profiling male tissues because of stronger phenotypes observed in males (**Fig 1B-E**). Samples were processed for library preparation using TruSeq RNA Library Preparation Kit (Illumina, San Diego, CA) for poly-A selection, fragmentation, and reverse transcription using random hexamer-primers to generate first-strand cDNA. Second-strand cDNA was generated using RNase H and DNA polymerases, and sequencing adapters were ligated using the Illumina Paired-End sample prep kit. Library products of 250-400bp fragments were isolated, amplified, and sequenced with Illumina Hiseq2500 System. After quality control using FastQC [46], the HISAT-StringTie pipeline [47] was used for sequence alignment and transcript assembly. Identification of differentially expressed genes (DEGs) were conducted using DEseq2 [48]. To account for multiple testing, we used the q-value method [49]. After excluding genes with extremely low expression levels (FPKM < 1), only DEGs demonstrating differential expression comparing the BPA and control groups per tissue at a false discovery rate (FDR) < 5% were used for biological pathway analysis, network analysis, and phenotypic data integration, as described below.

Reduced representation bisulfite sequencing (RRBS) and data analysis

We constructed RRBS libraries for 18 DNA samples from adipose, hypothalamus and liver tissues from male offspring (n = 3 per group per tissue from the same set of tissues chosen for transcriptome analysis described above). The DNA samples were quantified using the dsDNA BR assay (Qubit, Waltham, MA) and 100ng of DNA was used for library preparation. After digestion of the DNA with the MspI enzyme, samples underwent an end-repair and adenylation process, followed by adapter ligation using the Truseq barcode adapter (Illumina, San Diego, CA), size selection using AMPure Beads (Beckman Coulter, Brea, CA), and bisulfite treatment using the Epitect Kit (Qiagen, Germantown, MD). Bisulfite-treated DNA was then amplified using the Truseq Library Prep Kit (Illumina, San Diego, CA) and sequenced with the Illumina Hiseq2500 System. Bisulfite-converted reads were processed and aligned to the reference mouse genome (GRCm38/mm10 build) using the bisulfite aligner BSMAP [50]. We then used MOAB [51] for methylation ratio calling and identification of differentially methylated CpGs (DMCs). FDR was estimated using the q-value approach. Loci with methylation level changes of > 5% between BPA and control groups and FDR < 0.05 for each tissue were considered statistically significant DMCs. To annotate the locations of the identified DMCs in relation to gene regions and repetitive DNA elements accessed from UCSC genome browser, we used the Bioconductor package “annotatr” [52]. Specifically, gene regions were categorized into 1) 1-5kb upstream of the transcription start site (TSS), 2) promoter (< 1kb upstream of the TSS), 3) 5’ untranslated region (UTR), 4) exons, 5) introns, and 6) 3’UTR. The “annotatr” package was also used to annotate DMCs for known long non-coding RNAs (lncRNAs) based on GENCODE Release M16. Over-representation of DMCs within each category was calculated using Fisher’s exact test. We further evaluated the link between DEGs and their local DMCs (DMCs annotated as any of the 6 above mentioned gene regions) by correlating the methylation ratio of DMCs with the expression level of DEGs.

Pathway, network, and disease association analyses of DEGs and DMCs using the Mergeomics R package

To investigate the functional connections among the BPA-associated DEGs or DMCs (collectively referred to as molecular signatures of BPAs) and to assess the potential association of BPA affected genes with diseases in human populations, we utilized the Mergeomics package [53], an open-source bioconductor package (https://bioconductor.org/packages/devel/bioc/html/Mergeomics.html) designed to perform various integrative analyses in multi-omics studies. Mergeomics consists of two main libraries, Marker Set Enrichment Analysis (MSEA) and Weighted Key Driver Analysis (wKDA). In the current study, we used MSEA to assess 1) whether known biological processes, pathways or transcription factor targets were enriched for BPA molecular signatures as a means to annotate the potential functions or regulators of the molecular signatures, and 2) whether the BPA signatures demonstrate enrichment for disease associations identified in human genome-wide association studies (GWAS) of various complex diseases (**S1 Fig**). wKDA leverages gene network topology (interactions or regulatory relations among genes) and edge weight (strength or reliability of interactions and regulatory relations) information of graphical gene networks to predict potential key regulators of a given group of genes, in this case, the BPA-associated DEGs (**S2 Fig**). Both MSEA and wKDA were built around a chi-square like statistics (**S1 Text**) that yields robust findings that have been experimentally validated [41,42,53]. Details of each usage of the Mergeomics package are discussed below.

Functional annotation of DEGs and DMCs

To infer the functions of the DEGs and DMCs affected by BPA, we used MSEA to annotate the DEGs or local genes adjacent to the DMCs with known biological pathways curated from the Kyoto Encyclopedia of Genes and Genomes (KEGG) [54] and Reactome [55]. In brief, we extracted the differential expression p-values of genes in each pathway from the differential expression or methylation analyses and compared these p-values against the null distribution of p-values from random gene sets with matching gene numbers. If genes in a given pathway

collectively show more significant differential expression or differential methylation p-values compared to random genes based on a chi-square like statistic, we annotate the DEGs or DMCs using that pathway (**S1 Text**). DEGs and DMCs can have multiple over-represented pathways.

Identification of transcription factor (TF) hotspots perturbed by BPA

To dissect the regulatory cascades of BPA, we first assessed whether BPA-associated DEGs were downstream targets of specific transcription factors. The hypothesis behind this analysis is that BPA first affects TFs which in turn regulate the expression of downstream genes. We used TF regulatory networks for adipose, brain, and liver tissue retrieved from the FANTOM5 database [56]. Note that only a whole brain (instead of hypothalamus) TF network was available, which may only partially represent hypothalamic gene regulation. Each TF network was processed to keep the edges with high confidence (**S1 Text**). To identify TFs whose targets were perturbed by BPA, the downstream nodes of each TF in the network were pooled as the target genes for that TF. We then assessed the enrichment for BPA exposure related DEGs among the target genes of each TF using MSEA. TFs with FDR < 5% were considered statistically significant. Cytoscape software was used for TF network visualization [57].

Bayesian network and Weighted Key Driver Analysis (wKDA) to identify potential non-TF regulators

To further identify non-TF regulators that sense BPA and then perturb downstream genes, we used Bayesian networks (BN) of adipose, hypothalamus and liver tissues constructed from genetic and transcriptomic data from several large-scale mouse and human studies (**S1 Text and S1 Table**). wKDA was used to identify network key drivers (KDs), which are defined as network nodes whose neighboring subnetworks are significantly enriched for BPA-associated DEGs. Briefly, wKDA takes gene set G (i.e. BPA DEGs) and directional gene network N (i.e. BNs) as inputs. For every gene K in network N, neighboring genes within 1-edge distance were tested for

enrichment of genes in G using a chi-square like statistics followed by FDR assessment by permutation (**S1 Text and S2 Fig**). Network genes that reached FDR < 0.05 were reported as potential KDs.

Association of BPA DEGs and DMCs with mouse phenotypes and human diseases/traits

To assess whether the BPA molecular signatures were related to phenotypes examined in the mouse offspring, we calculated the Pearson correlation coefficient among expression level of DEGs, methylation ratio of DMCs, and the measurement of metabolic traits. For human diseases or traits, we accessed the GWAS catalog database [58] and collected the lists of candidate genes reported to be associated with 161 human traits/diseases ($P < 1e\text{-}5$). These genes were tested for enrichment of the BPA DEGs and DMCs in our mouse study using MSEA. We further curated all publicly available full summary statistics for 61 human traits/diseases from various public repositories (**S1 Text and S2 Table**). This allowed us to apply MSEA to comprehensively assess the enrichment for human disease association among BPA transcriptomic signatures using the full-spectrum of large-scale human GWAS. For each tissue-specific gene signature, we used the SNPs within a 50kb chromosomal distance as the representing SNPs for that gene. The trait/disease association p-values of the SNPs were then extracted from each GWAS and compared to the p-values of SNPs of random sets of genes to assess whether the BPA signatures were more likely to show stronger disease association in human GWAS (**S1 Text and S1 Fig**). This strategy has been successfully used in our previous animal model studies to assess the connection of genes affected by environmental perturbations such as diets and trauma to various human diseases [40,59].

Results

Prenatal BPA exposure induces intrauterine growth retardation (IUGR) and alterations in cardiometabolic phenotypes

We exposed pregnant C57BL/6 mice to BPA during gestation (day 1 to day 20 post-conception) at the dosage of 5mg/kg/day, and observed alterations in various metabolic phenotypes in the male and female offspring with prenatal BPA exposure at the weaning age. Compared with the control group, both male and female offspring from the BPA group showed significantly lower body weight, indicative of IUGR, a trait that is strongly associated with later life insulin resistance and obesity risk (**Fig 1B, D**). There were also significant decreases in serum lipid parameters and an increase in serum glucose level in males (**Fig 1C**), but not in females (**Fig 1E**). The decreases in the lipid parameters at this early developmental stage likely reflect the growth retardation phenotype observed and may provide feedback signals to predispose the exposed offspring to lipid dysregulation later in life. The phenotypic differences between BPA and control groups are not the results of litter effect, as offspring from different dams in each group showed similar patterns (**S3 Fig**).

Prenatal BPA exposure induces tissue-specific transcriptomic alterations in male weaning offspring

To explore the molecular basis underlying the potential health impact of prenatal BPA exposure, we collected three core tissues important for metabolism from male offspring at 3 weeks. We focus on males due to the stronger phenotypes observed. Hypothalamus is the central regulator of endocrine and metabolic systems, whereas liver and white adipose tissues are critical for energy and metabolic homeostasis. We used RNA-seq to profile the transcriptome, and identified 86, 93, and 855 differentially expressed genes (DEGs) in the adipose tissue, hypothalamus, and liver tissue respectively, at FDR < 0.05 (**Fig 2A, S3 Table**). This supports the ability of

prenatal BPA exposure to induce large-scale transcriptomic disruptions in offspring, with the impact appearing to be more prominent in liver. The DEGs were highly tissue-specific, with only 12 out of the 86 adipose DEGs and 16 out of the 93 hypothalamus DEGs being found in liver. Interestingly, the hypothalamic DEGs are predominantly up-regulated in the BPA group whereas the other two tissues did not show such direction bias (**S4 Table**). Only one gene, *Cyp51* (sterol 14-alpha demethylase), was shared across all three tissues but with different directional changes (upregulated in hypothalamus and liver, downregulated in adipose) (**Fig 2B**). The Cyp51 protein catalyzes metabolic reactions including cholesterol and steroid biosynthesis and biological oxidation [60]. Previously, this gene was also found to be critical regulator for testicular spermatogenesis [61]. The consistent alteration of *Cyp51* across tissues suggests that this gene is a general target of BPA, with the potential to alter functions related to cholesterol, hormone, and energy metabolism.

Functional annotation of DEGs in adipose, hypothalamus, and liver tissues

To better understand the biological implications of the BPA exposure related DEGs in individual tissues, we evaluated the enrichment of DEGs for known biological pathways and functional categories (**Fig 2C-E,** full results in **S5 Table**). We observed strong enrichment for pathways related to lipid metabolism (lipid transport, fatty acid metabolism, cholesterol biosynthesis) and energy metabolism (biological oxidation, TCA cycle) across all three tissues. Most of these pathways appeared to be upregulated in all three tissues, with the exception of downregulation of genes involved in biological oxidation in adipose tissue (**Fig 2C-E**). Individual tissues also showed perturbations of unique pathways: PPAR signaling and arachidonic acid pathways were altered in liver; extracellular matrix related processes were enriched among hypothalamic DEGs; core histone genes were upregulated in adipose DEGs (**Fig 2C-E**). In addition, triglyceride biosynthesis and glucose metabolism pathways were also moderately enriched among adipose DEGs, whereas few changes were seen for genes involved in adipocyte differentiation (**S4 Fig**).

Prenatal BPA exposure induces tissue-specific epigenetic alterations in male weaning offspring

Consistent with the observed gene expression disruptions at the transcriptomic level, we observed numerous methylomic alterations using RRBS, which characterizes DNA methylation states of millions of potential epigenetic sites at single base resolution. At FDR < 5%, 5136, 104, and 476 differentially methylated CpGs (DMCs) were found in adipose, hypothalamus, and liver tissues, respectively (**Fig 3A, S6 Table**). Interestingly, BPA induced local methylation changes in *Gm26917* and *Yam1*, two lncRNAs with no previously known link to BPA, consistently across three tissues (**Fig 3B**). The majority of the DMCs are located in intergenic regions (32% - 38%), followed by introns (31% - 37%) and exons (13% - 15%), but there is a paucity of DMCs in the promoter region (3% - 5%) (**S5 Fig**). Contrary to predictions that promoter regions may be more prone to epigenetic changes, we found that within-gene and intergenic methylation alterations in DNA methylation are more prevalent, a pattern consistently observed in previous epigenomic studies [40,62]. In addition, 5.0%, 8.6%, and 8.1% DMCs overlap with repetitive DNA elements in adipose, hypothalamus, and liver, respectively, recapitulating previous report of the interaction between BPA and repetitive DNA [63].

For DMCs that are located within or adjacent to genes, we further tested whether the local genes adjacent to those DMCs show enrichment for known functional categories. Unlike DEGs, top processes enriched for DMCs concentrated on intra- and extra-cellular communication and signaling related pathways such as axon guidance, extracellular matrix organization and NGF signaling (**Fig 3C**, **full results in S7 Table**). The affected genes in these processes are related to cellular structure, cell adhesion, and cell migration, indicating that these functions may be particularly vulnerable to BPA induced epigenetic modulation.

Potential regulatory role of DMCs in transcriptional regulation of BPA induced DEGs

To explore the role of DMCs in regulating DEGs, we evaluated the connection between transcriptome and methylome by correlating the expression level of DEGs with the methylation ratio of their local DMCs. For the DEGs in adipose, hypothalamus and liver tissue, we identified 42, 36, and 278 local DMCs whose methylation ratios were significantly correlated with the gene expression. At a global level, compared to non-DEGs, DEGs are more likely to contain local correlated DMCs (**S6 Fig**). A closer look into the expression-methylation correlation by different chromosomal regions further revealed a context dependent correlation pattern (**Fig 3D**). In adipose and liver, the 3-5% of DMCs in promoter regions tend to show significant enrichment for negative correlation with DEGs, whereas gene body methylations for DEGs are more likely to show significant enrichment for positive correlation with gene expression. In hypothalamus, however, positive correlations between DEGs and DMCs are more prevalent across different gene regions. In addition, liver DMCs within lncRNAs were uniquely enriched for negative correlation with lncRNA expression, although the lack of a reliable mouse lncRNA target database prevented us from further investigating whether downstream targets of the lncRNAs were enriched in the DEGs. Specific examples of DEGs showing significant correlation with local DMCs include adipose DEG *Slc25a1* (Solute Carrier Family 25 Member 1, involved in triglyceride biosynthesis), hypothalamic DEG *Mvk* (Mevalonate Kinase, involved in cholesterol biosynthesis), and liver DEG *Gm20319* (a lncRNA with unknown function) (**S7 Fig and S8 Table**). These results support a role of BPA-induced differential methylation in altering the expression levels of adjacent genes.

Pervasive influence of prenatal BPA exposure on the liver transcription factor network

BPA is known to bind to diverse types of nuclear receptors such as estrogen receptors and peroxisome proliferator-activated (PPAR) receptors that function as transcription factors (TFs), thus influencing the action of downstream genes [64,65]. *PPARg* in particular has been shown to be a target of BPA in mouse and human and

mechanistically linking BPA exposure with its associated effect on weight gain and increased adipogenesis [66-68]. To explore the TF regulatory landscape underlying BPA exposure based on our genome-wide data, we leveraged tissue-specific TF regulatory networks from the FANTOM5 project [56] and integrated it with our BPA transcriptome profiling data. No TF was found to be differentially expressed in adipose tissue, whereas 1 TF (Pou3f1) and 14 TFs (such as Esrra, Hnf1a, Pparg, Tcf21, Srebf1) were found to be differentially expressed in hypothalamus and liver, respectively. Due to the temporal nature of TF action, changes in TF levels may precede the downstream target genes and not be reflected in the transcriptomic profiles measured at the time of sacrifice. Therefore, we further curated the target genes of TFs from FANTOM5 networks and tested the enrichment for the target genes of each TF among our tissue-specific DEGs (**S9 Table**). This analysis confirmed that BPA perturbs the activity of the downstream targets for estrogen receptors Esrrg ($p = 1.4e-3$, FDR = 1.9%) and Esrra ($p = 0.03$, FDR = 13%) in liver, as well as Esr1 in both adipose ($p = 7.2e-3$, FDR = 10.6%) and liver ($p = 7.2e-3$, FDR = 4.7%). Targets of Pparg were also perturbed in liver ($p = 4.1e-3$, FDR = 3.8%). Therefore, we demonstrated that our data-driven network modeling is able to not only recapitulate results from previous *in-vitro* and *in-vivo* studies showing that BPA influences estrogen signaling and PPAR signaling [65], but also uniquely point to the tissue specificity of these BPA target TFs.

In addition to these expected TFs, we identified 14 adipose TFs and 61 liver TFs whose target genes were significantly enriched for BPA DEGs at FDR < 5%. Many of these TFs showed much stronger enrichment for BPA DEGs among their downstream targets than the estrogen receptors (**S9 Table**). The adipose TFs include nuclear transcription factor Y subunit alpha (Nfya) and fatty acid synthase (Fasn), both implicated in the adipocyte energy metabolism [69]. The liver TFs include multiple genes from the hepatocyte nuclear factors (HNF) family and the CCAAT-enhancer-binding proteins (CEBP) family, which are critical for liver development and function, suggesting a pervasive influence of BPA on liver TF regulation.

We further extracted the subnetwork containing 89 unique downstream targets of the significant liver TFs that are also liver DEGs. This subnetwork showed significant enrichment for genes involved in metabolic pathways such

as steroid hormone biosynthesis and fatty acid metabolism. The regulatory subnetwork for the top liver TFs (FDR < 5%) revealed a highly interconnected TF subnetwork that potentially senses BPA exposure and in turn governs the expression levels of their targets (**Fig 4A**), with *Pparg* and *Hnf4* among the core TFs. Some of the TFs in this network, including *Esr1*, *Esrrg*, *Foxp1*, and *Tcf7l1*, also had local DMCs identified in our study, indicating that BPA may perturb this liver TF subnetwork via local modification of DNA methylation of key TFs.

Identification of potential non-TF regulators governing BPA induced molecular perturbations

To further identify regulatory genes that mediate the action of BPA on downstream targets through non-TF mechanisms, we leveraged data-driven tissue-specific Bayesian networks (BNs) generated from multiple independent human and mouse studies (**S1 Table**). These data-driven networks are complementary to the TF networks used above and have proven valuable for accurately predicting gene-gene regulatory relationships and novel key drivers (KDs) [39-42,70]. KDs were defined as network nodes whose surrounding subnetworks are significantly enriched for BPA exposure related DEGs. At FDR < 1%, we identified 21, 1, and 100 KDs in adipose, hypothalamus, and liver, respectively (**S10 Table**). The top KDs in adipose (top 5 KDs *Acss2*, *Pc*, *Agpat2*, *Slc25a1*, *Acly*), hypothalamus (*Fa2h*) and liver (top 5 KDs *Dhcr7*, *Aldh3a2*, *Fdft1*, *Mtmr11*, *Hmgcr*) were involved in cholesterol, fatty acid and glucose metabolism processes. In addition, three KDs, *Acss2* (Acetyl-Coenzyme A Synthetase 2), *Acat2* (Acetyl-CoA Acetyltransferase 2), and *Fasn* (Fatty Acid Synthase), were involved in the upregulation of DEGs in both adipose and liver, despite the fact that few DEG signatures overlap across tissues (**Fig 4B**). These KDs are consistent with the observed increased expression of several genes implicated in lipogenesis, including *Fasn*, and help explain the liver accumulation of triglycerides when mice are exposed to BPA [71]. Together, these results indicate that BPA may engage certain common regulators which have tissue-specific targets. The distinct upregulatory pattern within the subnetworks of individual KDs supports the potential functional importance of KDs in orchestrating the action of downstream genes. These KDs, along

with the newly identified TFs from the above analysis, may represent novel regulatory targets which transmit the *in vivo* biological effects of BPA.

BPA transcriptomic and methylomic signatures are related to metabolic traits in mice

To assess the relationship between the BPA molecular signatures and metabolic traits in the mouse model, the DEGs and DMCs from individual tissues were tested for correlation with the measured metabolic traits: body weight, free fatty acids, total cholesterol, high density lipoprotein cholesterol, triglycerides and blood glucose. At $p < 0.05$, over two thirds of tissue-specific DEGs and over 60% DMCs were identified to be correlated with at least one metabolic trait (**Fig 5A, B**). Notably, liver DEGs exhibited stronger correlation with free fatty acid and triglycerides, whereas adipose DEGs were uniquely associated with glucose level, which is consistent with the pathway annotation results for these tissues. On the other hand, liver DMCs showed stronger correlations with metabolic traits than those from adipose and hypothalamus tissues.

Cross-examination of correlation across gene expression, DNA methylation, and metabolic traits revealed 35 consistent DEG-DMC-trait associations (3 in adipose, 4 in hypothalamus, and 28 in liver) (**S11 Table**). For example, in adipose tissue, *Fasn* (also a perturbed TF hotspot in adipose, and a shared KD in adipose and liver) was correlated with its exonic DMC at chr11:120816457, and both were correlated with triglyceride level; in hypothalamus, *Igf1r* (Insulin Like Growth Factor 1 Receptor) was correlated with its intronic DMC at chr7:68072768, and both were correlated with blood glucose level; in liver, *Adh1* (Alcohol Dehydrogenase 1A) was correlated with its intronic DMC at chr3:138287690, and both were correlated with body weight (**Fig 5C**). These results suggest that BPA alters local DMCs of certain genes to regulate gene expression, which may in turn regulate distinct metabolic traits.

Relevance of BPA signature to human complex traits/diseases

Human observational studies have associated developmental BPA exposure with a wide variety of human diseases ranging from cardiometabolic diseases to neuropsychiatric disorders [14,15,72]. Large-scale human genome-wide association studies offer an unbiased view of the genetic architecture for various human traits/diseases, and intersections of the molecular footprints of BPA in our mouse study with human disease risk genes can help infer the potential disease-causing properties of BPA in humans. From the GWAS Catalog [58], we collected associated genes for 161 human traits/diseases (traits with fewer than 50 associated genes were excluded), and evaluated the enrichment for the trait associated genes among DEG and DMC signatures. At FDR < 5%, no trait was found to be significantly enriched for BPA DEGs. Surprisingly, despite the difference between tissue-specific DMCs (**Fig 3B**), 19 out the 161 traits showed consistently strong enrichment for DMCs across all three tissues at FDR < 1%. The top traits include body mass index (BMI) and type 2 diabetes (**Table 1**). As DNA methylation status is known to determine long-term gene expression pattern instead of immediate dynamic gene regulation, the BMI and diabetes associated genes may be under long-term programming by BPA-induced differential methylation, thereby affecting later disease risks.

The above analysis involving the GWAS catalog focused only on small sets of the top candidate genes for various diseases and may have limited statistical power. To improve the statistical power, we curated the full summary statistics from 61 human GWAS that are publicly available (covering millions of SNP-trait associations in each GWAS), which enabled us to extend the assessment of disease association by considering additional human disease genes with moderate to low effect sizes (**Methods**). This analysis showed that DEGs from all three tissues exhibited consistent enrichment for genes associated with lipid traits such as triglycerides, LDL, and HDL **(Fig 6A-C**). Interestingly, enrichment for birth weight and birth length was also observed for hypothalamus and liver signatures, respectively. Liver DEGs were also significantly associated with coronary artery disease, inflammatory bowel disease, Alzheimer's disease, and schizophrenia. Top DEGs driving the inflammatory bowel disease association involve immune and inflammatory response genes (*PSMB9*, *TAP1*, *TNF*), whereas association

with Alzheimer's disease and schizophrenia involve genes related to cholesterol homeostasis (*APOA4*, *ABCG8*, *SOAT2*) and mitochondrial function (*GCDH*, *PDPR*, *SHMT2*), respectively. These results suggest that tissue-specific targets of BPA are connected to diverse human complex diseases through both the central nervous system and peripheral tissues.

Discussion

This multi-tissue, multi-omics integrative study represents one of the first systems biology investigations of prenatal BPA exposure. By integrating systematic profiling of the transcriptome and methylome of multiple metabolic tissues with phenotypic trait measurements, large-scale human association datasets, and network analysis, we uncovered insights into the molecular regulatory mechanisms underlying the health effect of prenatal BPA exposure. Specifically, we identified tens to hundreds of tissue-specific DEGs and DMCs involved in diverse biological functions such as metabolic pathways (oxidative phosphorylation/TCA cycle, fatty acid, cholesterol, glucose metabolism, and PPAR signaling), extracellular matrix, focal adhesion, and inflammation (arachidonic acid), with DMCs partially explaining the regulation of DEGs. Network analysis helped reveal potential regulatory circuits post BPA exposure and pinpointed both tissue-specific and cross-tissue regulators of BPA activities, including TFs such as estrogen receptors, *PPARg*, and *HNF1A*, and non-TF key drivers such as *FASN*. Furthermore, the BPA gene signatures and the predicted regulators were found to be linked to a wide spectrum of disease-related traits in both mouse and human.

The large-scale disruption we observed in the transcriptome and methylome in adipose and liver was consistent with previous reports [32,35,73,74]. For instance, comparison of our liver DEGs with the liver signatures identified from meta-analysis of available GEO datasets showed significant overlap (P = 8.2e-3 by Fisher's exact test, **See S1 Text**). However, our unique study design of examining multi-omics in multiple tissues in parallel yields higher comparability when integrating the results between data types and across tissues, as they were from

the same set of animals and were profiled in the same conditions. Furthermore, our advanced multidimensional integrative approach provides deeper insights into the regulatory cascades within and across tissues. Across all three tissues at the transcriptome level, we found that lipid metabolism and energy homeostasis related processes were consistently perturbed, with the scale of perturbation being strongest in liver. This aligns well with the significant changes in the plasma lipid profiles we observed in the offspring, the reported perturbation of lipid metabolism in fetal murine liver [74], and the reported susceptibility for nonalcoholic fatty liver diseases following BPA exposure [75-77]. The only shared gene across tissues, *Cyp51*, is involved in cholesterol and sterol biosynthesis and beta oxidation, again supporting that metabolism is a central target of BPA. At the methylome level, we are able to replicate 5 out of 7 peak hypomethylated genes, and 6 out of 9 peak hypermethylated genes from a study focusing on the gonadal adipose tissue [35]. We also revealed an intriguing link between BPA and lncRNAs across tissues, whose functional importance in developmental processes, disease progression, and response to BPA exposure was increasingly recognized yet underexplored [78]. Our molecular data provides intriguing lncRNA candidates such as *Gm20319*, *Gm26917*, and *Yam1* for future in-depth functional analyses.

For adipose tissue, clusters of genes responsible for core histones were found to be uniquely altered. Along with the strong adipose-specific differential methylation status, our results revealed gonadal adipose tissues as an especially vulnerable site for BPA induced epigenetic reprogramming. Besides, developmental BPA exposure has been previously suggested to influence white adipocyte differentiation [79-81]. However, the adipocyte differentiation pathway was not significantly enriched in our study. This is consistent with the report by Angel et al. [81], where increased adipocyte number is only found in mouse offspring with prenatal BPA exposure at 5ug/kg/day and 500ug/kg/day, but not 5mg/kg/day. Additionally, we found significant changes in triglyceride biosynthesis and glucose metabolism genes, suggesting that prenatal BPA exposure affects fat storage and glucose homeostasis in the adipose tissue. Although here we mainly investigate gonadal adipose tissue as a surrogate for abdominal fat in the context of metabolic disorders, the information may be useful for exploring the relationship between this fat depot and the gonad.

With regards to the hypothalamus, our study is the first to investigate the effect of BPA on the hypothalamic transcriptome and DNA methylome. Hypothalamus is an essential brain region that regulates the endocrine system, peripheral metabolism, and numerous brain functions. We identified BPA-induced DEGs and DMCs that were enriched for extracellular matrix related processes such as axon guidance, focal adhesion, and various metabolic processes. These hypothalamic pathways have been previously associated with metabolic [40,41] and neurodegenerative diseases [40,82], and they could underlie the reported disruption of hypothalamic melanocortin circuitry after BPA exposure [83]. Our study highlights the hypothalamus as another critical yet under-recognized target for BPA.

By interrogating both the transcriptome and DNA methylome in matching tissues, we were able to directly assess both global and specific correlative relationships between DEGs and DMCs (**S6 Fig, Fig 3D**). Specifically, we found that DEGs are more likely to have correlated DMCs in the matching tissue, a trend that persists in non-promoter regions. Our results corroborate previous findings regarding the importance of gene body methylation in disease etiology [84,85]. Given that over 90% of DMCs were found in non-promoter regions, closer investigation of the regulatory circuits involving these regions may unveil new insights into BPA response [62].

Known as an endocrine disrupting chemical, BPA has been speculated to exert its primary biological action by modifying the activity of hormone receptors, including estrogen receptors, PPARg and glucocorticoid receptors [65]. Indeed, the activity for the downstream targets of Pparg and three estrogen and estrogen-related receptors were found to be disrupted in liver by prenatal BPA exposure. More importantly, our unbiased data-driven analysis revealed many novel transcription factors and non-TF regulatory genes that also likely mediate BPA effects. In fact, many of the newly identified TF targets of BPA, such as Fasn and several hepatic nuclear factors, showed much higher ranking in our regulator prediction analyses. In liver, a tightly inter-connected TF subnetwork was highly concentrated with BPA affected genes involved in metabolic processes such as cytochrome P450 system (*Cyp3a25, Cyp2a12, Cyp1a2*), lipid (*Apoa4, Abcg5, Soat2*) and glucose (*Hnf1a, Adra1b, Gck*) regulation, with extensive footprints of altered methylation status in the TFs and other subnetwork

genes (**Fig 4A**). Therefore, our results support a widespread impact of BPA on liver transcriptional regulation, and the convergence of differential methylation and gene expression in this TF subnetwork implies that BPA perturbs this subnetwork via epigenetic regulation of the TFs, which in turn trigger transcriptomic alterations in downstream genes. In adipose, we discovered a regulatory axis governed by Nfya and Fasn that are known regulators of fatty acid metabolism and adipogenesis. NF-YA is a histone-fold domain protein that binds to the inverted CCAAT element in the *Fasn* promoter [69,86], and both *Nfya* and *Fasn* were found to significantly perturbed by BPA in our study. Moreover, *Fasn* also serves as a cross-tissue KD, governing distinct groups of up-regulated lipid metabolism genes in adipose and liver post-BPA exposure (**Fig 4B**), supporting its role in mediating the BPA-induced lipid dysregulation at the systemic level. The significant correlation of gene expression and methylation for *Fasn* with triglyceride level furthers implicates its role as a network-level regulator and biomarker for BPA induced lipid dysregulation. Our observation of *Fasn* is consistent with evidences suggesting its susceptibility to methylation perturbation under obesogenic feeding [87] and its causal functional importance for fatty liver diseases [42,88]. These novel regulators warrant future experimental testing of their causal regulatory role in BPA activities via genetic manipulation studies, such as knocking down or overexpressing *Fasn* to examine the modulation of BPA activities.

One unique aspect of this study is the linking of the molecular landscape of prenatal BPA exposure to traits/diseases in both mouse and human. In our mouse study, the observed changes in body weight, lipid profiles, and glucose level are highly concordant with the functions of the molecular targets. For instance, prenatal BPA exposure perturbs both the expression levels and the local DNA methylation status of *Fasn*, *Igf1r*, and *Adh1*. These DEGs and their local DMCs also significantly correlate with phenotypic outcomes, thus serving as examples of how DNA methylation and gene regulation bridge the gap between BPA exposure and phenotypic manifestation. To further enhance the translatability of our findings from mouse to human, we searched for human diseases linked to the BPA-affected genes. An intriguing discovery is the prominent overrepresentation of differential methylation signals in adipose, hypothalamus, and liver within known genes related to obesity and

type 2 diabetes, supporting that BPA may impact obesity and diabetes risk through systemic reprogramming of DNA methylation. More sophisticated analysis incorporating the BPA differential gene expression and the full statistics of human genome-wide association studies corroborated the observed connection between prenatal BPA exposure and lipid homeostasis [89], birth weight [90], and coronary artery disease [14] reported in observational studies. Moreover, our findings suggest the involvement of prenatal BPA exposure in the development of inflammatory bowel syndrome, schizophrenia, and Alzheimer's disease. These associations warrant future investigations.

One limitation of our work is the restriction of study scope to weaning age male mice with *in utero* BPA exposure below the NOAEL (5mg/kg/d) as a proof-of-concept for our systems biology framework. Considering that the effects of early-life exposure to BPA is highly variable and dependent on factors such as the dose, window, route, and frequency of exposure as well as genetic background, age, and sex [13], future studies testing these additional variables are necessary to generate a comprehensive understandings of BPA risks under various exposure conditions.

Conclusions

Our study represents the first multi-tissue, multi-omics integrative investigation of prenatal BPA exposure. The systems biology framework we applied revealed how BPA triggers cascades of regulatory circuits involving numerous transcription factors and non-TF regulators that coordinate diverse molecular processes within and across core metabolic tissues, thereby highlighting that BPA exerts its biological functions via much more diverse targets than previously thought. As such, our findings offer a comprehensive systems-level understanding of tissue sensitivity and molecular perturbations elicited by prenatal BPA exposure, and offer promising novel candidates for targeted mechanistic investigation as well as much-needed network-level biomarkers of prior BPA exposure. The strong influence of BPA on metabolic pathways and cardiometabolic phenotypes merits it characterization as a general metabolic disruptor posing systemic health risks.

Acknowledgments

LS is supported by UCLA Dissertation Year Fellowship, Eureka Scholarship, Hyde Scholarship, Burroughs Wellcome Fund Inter-School Program in Metabolic Diseases Fellowship, and China Scholarship Council. XY is supported by NIH DK104363 and NS103088, and Leducq Foundation. We would also like to thank Zhe Ying's assistance in collecting mice hypothalamus tissue, and Dr. Guanglin Zhang's assistance in the RRBS experiments.

Competing interests

The authors declare that they have no competing interest.

References

1. Barouki R, Gluckman PD, Grandjean P, Hanson M, Heindel JJ (2012) Developmental origins of non-communicable disease: implications for research and public health. Environ Health 11: 42.

2. Boekelheide K, Blumberg B, Chapin RE, Cote I, Graziano JH, et al. (2012) Predicting later-life outcomes of early-life exposures. Environ Health Perspect 120: 1353-1361.

3. Heindel JJ, Vandenberg LN (2015) Developmental origins of health and disease: a paradigm for understanding disease etiology and prevention. Current opinion in pediatrics 27: 248.

4. Vandenberg LN, Hauser R, Marcus M, Olea N, Welshons WV (2007) Human exposure to bisphenol A (BPA). Reprod Toxicol 24: 139-177.

5. Tsai WT (2006) Human health risk on environmental exposure to Bisphenol-A: a review. J Environ Sci Health C Environ Carcinog Ecotoxicol Rev 24: 225-255.

6. Sun C, Leong LP, Barlow PJ, Chan SH, Bloodworth BC (2006) Single laboratory validation of a method for the determination of Bisphenol A, Bisphenol A diglycidyl ether and its derivatives in canned foods by reversed-phase liquid chromatography. J Chromatogr A 1129: 145-148.

7. Calafat AM, Ye X, Wong LY, Reidy JA, Needham LL (2008) Exposure of the U.S. population to bisphenol A and 4-tertiary-octylphenol: 2003-2004. Environ Health Perspect 116: 39-44.

8. Rubin BS, Paranjpe M, DaFonte T, Schaeberle C, Soto AM, et al. (2017) Perinatal BPA exposure alters body weight and composition in a dose specific and sex specific manner: The addition of peripubertal exposure exacerbates adverse effects in female mice. Reprod Toxicol 68: 130-144.

9. Hao M, Ding L, Xuan L, Wang T, Li M, et al. (2017) Urinary bisphenol A concentration and the risk of central obesity in Chinese adults: A prospective study. J Diabetes.

10. Beydoun HA, Khanal S, Zonderman AB, Beydoun MA (2014) Sex differences in the association of urinary bisphenol-A concentration with selected indices of glucose homeostasis among U.S. adults. Ann Epidemiol 24: 90-97.

11. Teppala S, Madhavan S, Shankar A (2012) Bisphenol A and Metabolic Syndrome: Results from NHANES. Int J Endocrinol 2012: 598180.

12. Mouneimne Y, Nasrallah M, Khoueiry-Zgheib N, Nasreddine L, Nakhoul N, et al. (2017) Bisphenol A urinary level, its correlates, and association with cardiometabolic risks in Lebanese urban adults. Environ Monit Assess 189: 517.

13. Wassenaar PNH, Trasande L, Legler J (2017) Systematic Review and Meta-Analysis of Early-Life Exposure to Bisphenol A and Obesity-Related Outcomes in Rodents. Environ Health Perspect 125: 106001.

14. Han C, Hong YC (2016) Bisphenol A, Hypertension, and Cardiovascular Diseases: Epidemiological, Laboratory, and Clinical Trial Evidence. Curr Hypertens Rep 18: 11.

15. Ranciere F, Lyons JG, Loh VH, Botton J, Galloway T, et al. (2015) Bisphenol A and the risk of cardiometabolic disorders: a systematic review with meta-analysis of the epidemiological evidence. Environ Health 14: 46.

16. Liu J, Yu P, Qian W, Li Y, Zhao J, et al. (2013) Perinatal bisphenol A exposure and adult glucose homeostasis: identifying critical windows of exposure. PLoS One 8: e64143.

17. Ryan KK, Haller AM, Sorrell JE, Woods SC, Jandacek RJ, et al. (2010) Perinatal exposure to bisphenol-a and the development of metabolic syndrome in CD-1 mice. Endocrinology 151: 2603-2612.

18. Miyawaki J, Sakayama K, Kato H, Yamamoto H, Masuno H (2007) Perinatal and postnatal exposure to bisphenol a increases adipose tissue mass and serum cholesterol level in mice. J Atheroscler Thromb 14: 245-252.

19. Rubin BS, Soto AM (2009) Bisphenol A: Perinatal exposure and body weight. Mol Cell Endocrinol 304: 55-62.

20. Garcia-Arevalo M, Alonso-Magdalena P, Rebelo Dos Santos J, Quesada I, Carneiro EM, et al. (2014) Exposure to bisphenol-A during pregnancy partially mimics the effects of a high-fat diet altering glucose homeostasis and gene expression in adult male mice. PLoS One 9: e100214.

599 21. Manikkam M, Tracey R, Guerrero-Bosagna C, Skinner MK (2013) Plastics derived endocrine disruptors
600 (BPA, DEHP and DBP) induce epigenetic transgenerational inheritance of obesity, reproductive disease and
601 sperm epimutations. PLoS One 8: e55387.
602 22. Susiarjo M, Xin F, Bansal A, Stefaniak M, Li C, et al. (2015) Bisphenol a exposure disrupts metabolic health
603 across multiple generations in the mouse. Endocrinology 156: 2049-2058.
604 23. Bansal A, Rashid C, Xin F, Li C, Polyak E, et al. (2017) Sex- and Dose-Specific Effects of Maternal
605 Bisphenol A Exposure on Pancreatic Islets of First- and Second-Generation Adult Mice Offspring. Environ
606 Health Perspect 125: 097022.
607 24. Baillie-Hamilton PF (2002) Chemical toxins: a hypothesis to explain the global obesity epidemic. J Altern
608 Complement Med 8: 185-192.
609 25. Heindel JJ (2003) Endocrine disruptors and the obesity epidemic. Toxicol Sci 76: 247-249.
610 26. Newbold RR, Padilla-Banks E, Jefferson WN, Heindel JJ (2008) Effects of endocrine disruptors on obesity.
611 Int J Androl 31: 201-208.
612 27. EFS Authority (2015) Scientific opinion on the risks to public health related to the presence of bisphenol A
613 (BPA) in foodstuffs. EFSA Journal 13.
614 28. Beronius A, Johansson N, Ruden C, Hanberg A (2013) The influence of study design and sex-differences on
615 results from developmental neurotoxicity studies of bisphenol A: implications for toxicity testing. Toxicology
616 311: 13-26.
617 29. Ariemma F, D'Esposito V, Liguoro D, Oriente F, Cabaro S, et al. (2016) Low-Dose Bisphenol-A Impairs
618 Adipogenesis and Generates Dysfunctional 3T3-L1 Adipocytes. PLoS One 11: e0150762.
619 30. Ben-Jonathan N, Hugo ER, Brandebourg TD (2009) Effects of bisphenol A on adipokine release from human
620 adipose tissue: Implications for the metabolic syndrome. Mol Cell Endocrinol 304: 49-54.
621 31. Olsvik PA, Skjaerven KH, Softeland L (2017) Metabolic signatures of bisphenol A and genistein in Atlantic
622 salmon liver cells. Chemosphere 189: 730-743.

623 32. Lejonklou MH, Dunder L, Bladin E, Pettersson V, Ronn M, et al. (2017) Effects of Low-Dose Developmental
624 Bisphenol A Exposure on Metabolic Parameters and Gene Expression in Male and Female Fischer 344 Rat
625 Offspring. Environ Health Perspect 125: 067018.
626 33. Anderson OS, Kim JH, Peterson KE, Sanchez BN, Sant KE, et al. (2017) Novel Epigenetic Biomarkers
627 Mediating Bisphenol A Exposure and Metabolic Phenotypes in Female Mice. Endocrinology 158: 31-40.
628 34. Ma Y, Xia W, Wang DQ, Wan YJ, Xu B, et al. (2013) Hepatic DNA methylation modifications in early
629 development of rats resulting from perinatal BPA exposure contribute to insulin resistance in adulthood.
630 Diabetologia 56: 2059-2067.
631 35. Taylor JA, Shioda K, Mitsunaga S, Yawata S, Angle BM, et al. (2017) Prenatal Exposure to Bisphenol A
632 Disrupts Naturally Occurring Bimodal DNA Methylation at Proximal Promoter of fggy, an Obesity-relevant Gene
633 Encoding a Carbohydrate Kinase, in Gonadal White Adipose Tissues of CD-1 Mice. Endocrinology.
634 36. Faulk C, Kim JH, Jones TR, McEachin RC, Nahar MS, et al. (2015) Bisphenol A-associated alterations in
635 genome-wide DNA methylation and gene expression patterns reveal sequence-dependent and non-monotonic
636 effects in human fetal liver. Environ Epigenet 1.
637 37. Nahar MS, Kim JH, Sartor MA, Dolinoy DC (2014) Bisphenol A-associated alterations in the expression and
638 epigenetic regulation of genes encoding xenobiotic metabolizing enzymes in human fetal liver. Environ Mol
639 Mutagen 55: 184-195.
640 38. Messerlian C, Martinez RM, Hauser R, Baccarelli AA (2017) 'Omics' and endocrine-disrupting chemicals—
641 new paths forward. Nature Reviews Endocrinology 13: 740.
642 39. Makinen VP, Civelek M, Meng Q, Zhang B, Zhu J, et al. (2014) Integrative genomics reveals novel molecular
643 pathways and gene networks for coronary artery disease. PLoS Genet 10: e1004502.
644 40. Meng Q, Ying Z, Noble E, Zhao Y, Agrawal R, et al. (2016) Systems Nutrigenomics Reveals Brain Gene
645 Networks Linking Metabolic and Brain Disorders. EBioMedicine 7: 157-166.

41. Shu L, Chan KHK, Zhang G, Huan T, Kurt Z, et al. (2017) Shared genetic regulatory networks for cardiovascular disease and type 2 diabetes in multiple populations of diverse ethnicities in the United States. PLoS Genet 13: e1007040.

42. Krishnan KC, Kurt Z, Barrere-Cain R, Sabir S, Das A, et al. (2018) Integration of Multi-omics Data from Mouse Diversity Panel Highlights Mitochondrial Dysfunction in Non-alcoholic Fatty Liver Disease. Cell Systems.

43. Dolinoy DC, Huang D, Jirtle RL (2007) Maternal nutrient supplementation counteracts bisphenol A-induced DNA hypomethylation in early development. Proc Natl Acad Sci U S A 104: 13056-13061.

44. Susiarjo M, Sasson I, Mesaros C, Bartolomei MS (2013) Bisphenol a exposure disrupts genomic imprinting in the mouse. PLoS Genet 9: e1003401.

45. Bromer JG, Zhou Y, Taylor MB, Doherty L, Taylor HS (2010) Bisphenol-A exposure in utero leads to epigenetic alterations in the developmental programming of uterine estrogen response. FASEB J 24: 2273-2280.

46. Andrews S (2010) FastQC: a quality control tool for high throughput sequence data.

47. Pertea M, Kim D, Pertea GM, Leek JT, Salzberg SL (2016) Transcript-level expression analysis of RNA-seq experiments with HISAT, StringTie and Ballgown. Nat Protoc 11: 1650-1667.

48. Love MI, Huber W, Anders S (2014) Moderated estimation of fold change and dispersion for RNA-seq data with DESeq2. Genome Biol 15: 550.

49. Storey JD, Tibshirani R (2003) Statistical significance for genomewide studies. Proc Natl Acad Sci U S A 100: 9440-9445.

50. Xi Y, Li W (2009) BSMAP: whole genome bisulfite sequence MAPping program. BMC Bioinformatics 10: 232.

51. Sun D, Xi Y, Rodriguez B, Park HJ, Tong P, et al. (2014) MOABS: model based analysis of bisulfite sequencing data. Genome Biol 15: R38.

52. Cavalcante RG, Sartor MA (2017) annotatr: genomic regions in context. Bioinformatics 33: 2381-2383.

53. Shu L, Zhao Y, Kurt Z, Byars SG, Tukiainen T, et al. (2016) Mergeomics: multidimensional data integration to identify pathogenic perturbations to biological systems. BMC Genomics 17: 874.

54. Kanehisa M, Goto S (2000) KEGG: kyoto encyclopedia of genes and genomes. Nucleic Acids Res 28: 27-30.

55. Croft D, Mundo AF, Haw R, Milacic M, Weiser J, et al. (2014) The Reactome pathway knowledgebase. Nucleic Acids Res 42: D472-477.

56. Marbach D, Lamparter D, Quon G, Kellis M, Kutalik Z, et al. (2016) Tissue-specific regulatory circuits reveal variable modular perturbations across complex diseases. Nat Methods 13: 366-370.

57. Shannon P, Markiel A, Ozier O, Baliga NS, Wang JT, et al. (2003) Cytoscape: a software environment for integrated models of biomolecular interaction networks. Genome Res 13: 2498-2504.

58. Welter D, MacArthur J, Morales J, Burdett T, Hall P, et al. (2014) The NHGRI GWAS Catalog, a curated resource of SNP-trait associations. Nucleic Acids Res 42: D1001-1006.

59. Meng Q, Zhuang Y, Ying Z, Agrawal R, Yang X, et al. (2017) Traumatic Brain Injury Induces Genome-Wide Transcriptomic, Methylomic, and Network Perturbations in Brain and Blood Predicting Neurological Disorders. EBioMedicine 16: 184-194.

60. Lewinska M, Juvan P, Perse M, Jeruc J, Kos S, et al. (2014) Hidden disease susceptibility and sexual dimorphism in the heterozygous knockout of Cyp51 from cholesterol synthesis. PLoS One 9: e112787.

61. Keber R, Rozman D, Horvat S (2013) Sterols in spermatogenesis and sperm maturation. J Lipid Res 54: 20-33.

62. Lou S, Lee HM, Qin H, Li JW, Gao Z, et al. (2014) Whole-genome bisulfite sequencing of multiple individuals reveals complementary roles of promoter and gene body methylation in transcriptional regulation. Genome Biol 15: 408.

63. Faulk C, Kim JH, Anderson OS, Nahar MS, Jones TR, et al. (2016) Detection of differential DNA methylation in repetitive DNA of mice and humans perinatally exposed to bisphenol A. Epigenetics 11: 489-500.

64. Acconcia F, Pallottini V, Marino M (2015) Molecular Mechanisms of Action of BPA. Dose Response 13: 1559325815610582.

65. MacKay H, Abizaid A (2017) A plurality of molecular targets: The receptor ecosystem for bisphenol-A (BPA). Horm Behav.

66. Wang J, Sun B, Hou M, Pan X, Li X (2013) The environmental obesogen bisphenol A promotes adipogenesis by increasing the amount of 11beta-hydroxysteroid dehydrogenase type 1 in the adipose tissue of children. Int J Obes (Lond) 37: 999-1005.

67. Ahmed S, Atlas E (2016) Bisphenol S- and bisphenol A-induced adipogenesis of murine preadipocytes occurs through direct peroxisome proliferator-activated receptor gamma activation. Int J Obes (Lond) 40: 1566-1573.

68. Vafeiadi M, Roumeliotaki T, Myridakis A, Chalkiadaki G, Fthenou E, et al. (2016) Association of early life exposure to bisphenol A with obesity and cardiometabolic traits in childhood. Environ Res 146: 379-387.

69. Nishi-Tatsumi M, Yahagi N, Takeuchi Y, Toya N, Takarada A, et al. (2017) A key role of nuclear factor Y in the refeeding response of fatty acid synthase in adipocytes. FEBS Lett 591: 965-978.

70. Zhang B, Gaiteri C, Bodea LG, Wang Z, McElwee J, et al. (2013) Integrated systems approach identifies genetic nodes and networks in late-onset Alzheimer's disease. Cell 153: 707-720.

71. Marmugi A, Ducheix S, Lasserre F, Polizzi A, Paris A, et al. (2012) Low doses of bisphenol A induce gene expression related to lipid synthesis and trigger triglyceride accumulation in adult mouse liver. Hepatology 55: 395-407.

72. Inadera H (2015) Neurological Effects of Bisphenol A and its Analogues. Int J Med Sci 12: 926-936.

73. Kim JH, Sartor MA, Rozek LS, Faulk C, Anderson OS, et al. (2014) Perinatal bisphenol A exposure promotes dose-dependent alterations of the mouse methylome. BMC Genomics 15: 30.

74. Ilagan Y, Mamillapalli R, Goetz LG, Kayani J, Taylor HS (2017) Bisphenol-A exposure in utero programs a sexually dimorphic estrogenic state of hepatic metabolic gene expression. Reprod Toxicol 71: 84-94.

716 75. Ke Z, Pan J, Jin L, Xu H, Yu T, et al. (2016) Bisphenol A exposure may induce hepatic lipid accumulation via
717 reprogramming the DNA methylation patterns of genes involved in lipid metabolism. Scientific reports 6.
718 76. Yang S, Zhang A, Li T, Gao R, Peng C, et al. (2017) Dysregulated Autophagy in Hepatocytes Promotes
719 Bisphenol A-Induced Hepatic Lipid Accumulation in Male Mice. Endocrinology 158: 2799-2812.
720 77. Shimpi PC, More VR, Paranjpe M, Donepudi AC, Goodrich JM, et al. (2017) Hepatic Lipid Accumulation
721 and Nrf2 Expression following Perinatal and Peripubertal Exposure to Bisphenol A in a Mouse Model of
722 Nonalcoholic Liver Disease. Environ Health Perspect 125: 087005.
723 78. Karlsson O, Baccarelli AA (2016) Environmental Health and Long Non-coding RNAs. Curr Environ Health
724 Rep 3: 178-187.
725 79. Somm E, Schwitzgebel VM, Toulotte A, Cederroth CR, Combescure C, et al. (2009) Perinatal exposure to
726 bisphenol a alters early adipogenesis in the rat. Environ Health Perspect 117: 1549-1555.
727 80. Vom Saal FS, Nagel SC, Coe BL, Angle BM, Taylor JA (2012) The estrogenic endocrine disrupting chemical
728 bisphenol A (BPA) and obesity. Mol Cell Endocrinol 354: 74-84.
729 81. Angle BM, Do RP, Ponzi D, Stahlhut RW, Drury BE, et al. (2013) Metabolic disruption in male mice due to
730 fetal exposure to low but not high doses of bisphenol A (BPA): evidence for effects on body weight, food intake,
731 adipocytes, leptin, adiponectin, insulin and glucose regulation. Reprod Toxicol 42: 256-268.
732 82. Vercruysse P, Vieau D, Blum D, Petersen A, Dupuis L (2018) Hypothalamic alterations in neurodegenerative
733 diseases and their relation to abnormal energy metabolism. Frontiers in Molecular Neuroscience 11: 2.
734 83. MacKay H, Patterson ZR, Abizaid A (2017) Perinatal Exposure to Low-Dose Bisphenol-A Disrupts the
735 Structural and Functional Development of the Hypothalamic Feeding Circuitry. Endocrinology 158: 768-777.
736 84. Jones PA (2012) Functions of DNA methylation: islands, start sites, gene bodies and beyond. Nat Rev Genet
737 13: 484-492.
738 85. Patil V, Ward RL, Hesson LB (2014) The evidence for functional non-CpG methylation in mammalian cells.
739 Epigenetics 9: 823-828.

740 86. Oldfield AJ, Yang P, Conway AE, Cinghu S, Freudenberg JM, et al. (2014) Histone-fold domain protein NF-
741 Y promotes chromatin accessibility for cell type-specific master transcription factors. Mol Cell 55: 708-722.
742 87. Gracia A, Elcoroaristizabal X, Fernandez-Quintela A, Miranda J, Bediaga NG, et al. (2014) Fatty acid
743 synthase methylation levels in adipose tissue: effects of an obesogenic diet and phenol compounds. Genes Nutr 9:
744 411.
745 88. Hui ST, Parks BW, Org E, Norheim F, Che N, et al. (2015) The genetic architecture of NAFLD among inbred
746 strains of mice. Elife 4.
747 89. Dallio M, Masarone M, Errico S, Gravina A, Nicolucci C, et al. (2018) Role of bisphenol A as environmental
748 factor in the promotion of non-alcoholic fatty liver disease: in vitro and clinical study. Alimentary pharmacology
749 & therapeutics.
750 90. Veiga-Lopez A, Kannan K, Liao C, Ye W, Domino SE, et al. (2015) Gender-Specific Effects on Gestational
751 Length and Birth Weight by Early Pregnancy BPA Exposure. J Clin Endocrinol Metab 100: E1394-1403.
752

Supporting information captions

S1 Text. Supplemental Methods.

S1 Fig. Schematic illustration of MSEA

S2 Fig. Schematic illustration (A) and key driver identification algorithms (B) of wKDA.

S3 Fig. Body weight of male and female offspring mice at weaning age by litters. Red arrows indicate offspring male mice selected for molecular profiling.

S4 Fig. Prenatal BPA exposure induced expression change for genes from the adipocyte differentiation, triglyceride biosynthesis, glucose metabolism, and core histone genes in the adipose tissue. P-values for enrichment of pathway genes among DEGs (shown in parenthesis in each panel heading) were determined by MSEA. *$p < 0.05$ in differential expression tests for individual genes by DEseq2; **FDR < 5% in differential expression tests for individual genes by DEseq2.

S5 Fig. Gene body location distribution for hyper- and hypo- methylated DMC s in adipose, hypothalamus, and liver.

S6 Fig. Quantile-quantile plots for the absolute Pearson correlation with local DMC for DEGs and Non DEGs in adipose, hypothalamus, and liver tissue. Statistical difference of the distribution of correlation value between DEGs (FDR < 5%) and non DEGs is determined by the Kolmogorov–Smirnov test.

S7 Fig. Scatter plots of correlations between DEG expression levels and DMC methylation ratios for *Slc25a1* in adipose, *Mvk* in hypothalamus, and *Gm20319* in liver.

S1 Table. Data resources and references for the construction of Bayesian gene-gene regulatory networks.

S2 Table. Source of publicly available full summary-level statistics from human genome-wide association studies.

S3 Table. List of DEGs with $p < 0.05$ in adipose, hypothalamus and liver tissue following prenatal exposure to BPA.

S4 Table. Count of DEGs in adipose, hypothalamus and liver tissue following prenatal exposure to BPA.

S5 Table. Results of functional annotation of DEGs in in adipose, hypothalamus and liver tissue following prenatal exposure to BPA

S6 Table. Count of differentially methylated regions in hypothalamus and liver tissue following prenatal exposure to BPA.

S7 Table. Results of functional annotation of DMCs in in adipose, hypothalamus and liver tissue following prenatal exposure to BPA.

S8 Table. List of pairs of DEGs and local DMCs with significant correlation ($p < 0.05$) in expression level and methylation ratio

S9 Table. List of transcription factors whose downstream targets were significantly enriched for DEGs ($p < 0.05$).

S10 Table. List of tissue-specific key drivers with FDR < 1%

S11 Table. List of DEGs with significant correlation between expression level, methylation ratio of local DMCs, and cardiometabolic traits ($p < 0.05$).

Tables

Table 1. Top 5 human traits whose associated genes in genome-wide association studies are enriched for differentially methylated CpGs (DMCs) across adipose, hypothalamus and liver at FDR < 1% in MSEA.

Human trait	Adipose		Hypothalamus		Liver	
	P	FDR	P	FDR	P	FDR
Obesity-related traits	1.28E-16	0.00%	3.03E-15	0.00%	2.71E-19	0.00%
Body mass index	1.30E-13	0.00%	3.74E-07	0.00%	9.66E-12	0.00%
Post bronchodilator FEV1/FVC ratio	8.17E-09	0.00%	1.45E-08	0.00%	3.67E-07	0.00%
Type 2 diabetes	1.21E-05	0.03%	8.97E-09	0.00%	0.001243	0.92%
Platelet distribution width	8.16E-08	0.00%	7.62E-05	0.16%	5.20E-05	0.12%

Figures

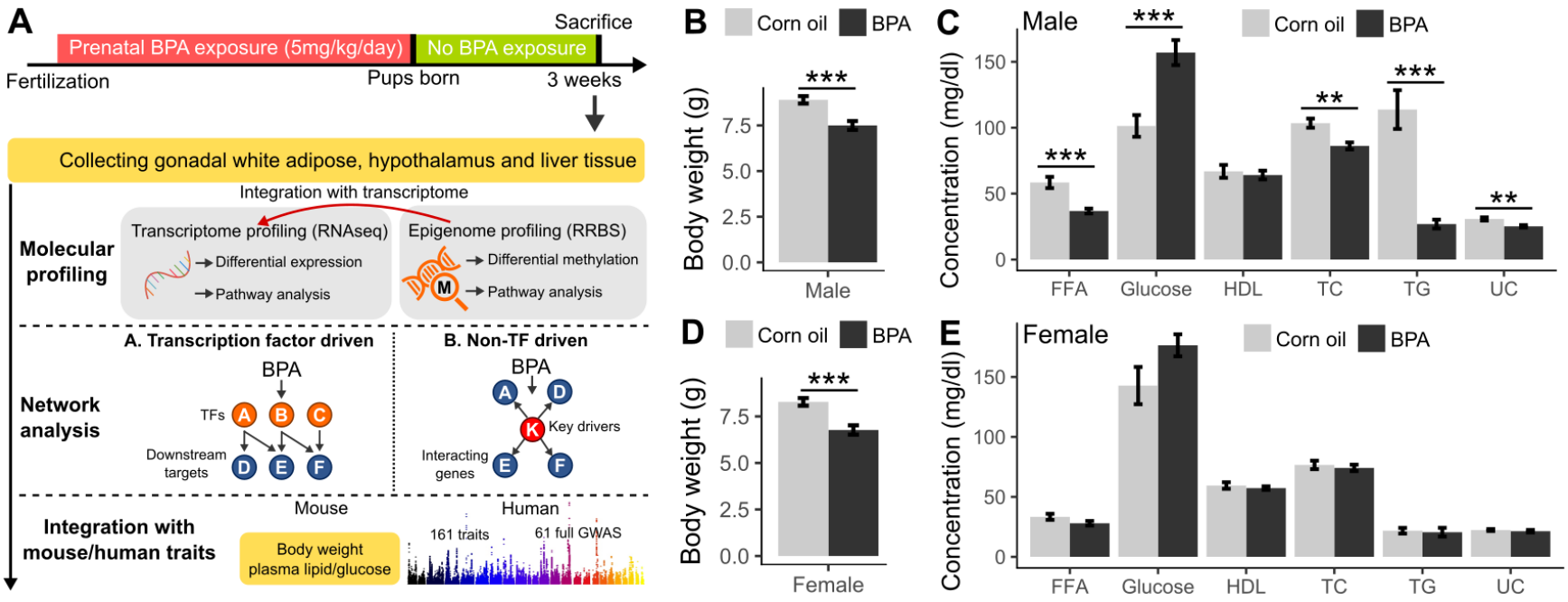

Fig 1. Overall study design and the measurements of metabolic traits in male and female offspring. (A) Framework of multi-omics approaches to investigate the impact of prenatal BPA exposure. B-C) Comparison of body weight, serum lipids and glucose level in male mice at weaning age. D-E) Comparison of body weight, serum lipids and glucose level in female mice at weaning age. FFA: free fatty acid; HDL: high-density lipoprotein cholesterol; TC: total cholesterol; TG: triglyceride; UC: unesterified cholesterol. * $p < 0.05$, ** $p < 0.01$, *** $p < 0.001$ by two-sided Student's T-test. N=9-13 mice/group.

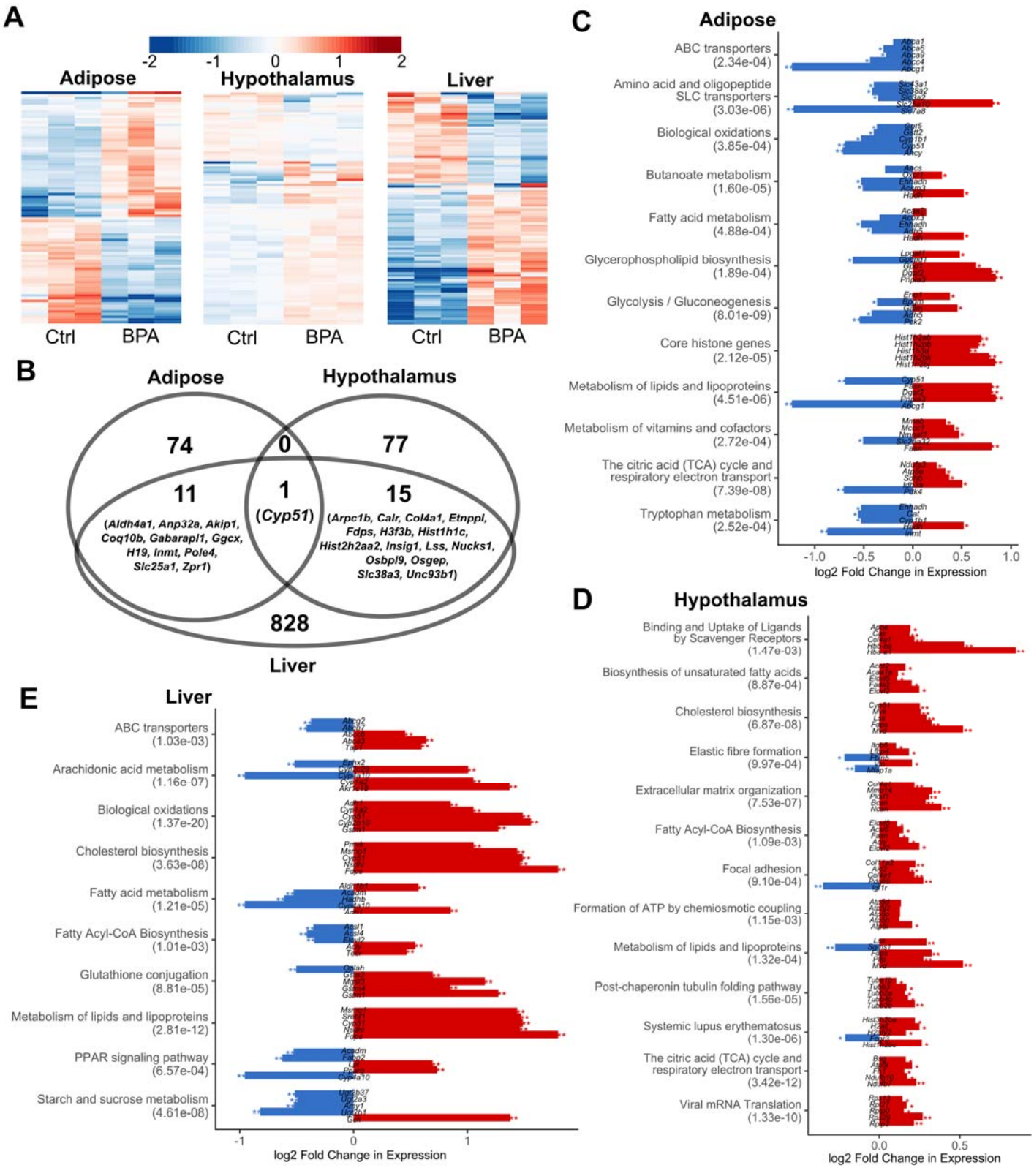
A
-2
-1
0
1
2
Adipose
Hypothalamus
Liver
Ctrl
BPA
Ctrl
BPA
Ctrl
BPA
B
Adipose
Hypothalamus
74
0
77
11
(Aldh4a1, Anp32a, Akip1, Coq10b, Gabarapl1, Ggcx, H19, Inmt, Pole4, Slc25a1, Zpr1)
1
(Cyp51)
15
(Arpc1b, Calr, Col4a1, Etnppl, Fdps, H3f3b, Hist1h1c, Hist2h2aa2, Insig1, Lss, Nucks1, Osbpl9, Osgep, Slc38a3, Unc93b1)
828
Liver
C
Adipose
ABC transporters (2.34e-04)
Amino acid and oligopeptide SLC transporters (3.03e-06)
Biological oxidations (3.85e-04)
Butanoate metabolism (1.60e-05)
Fatty acid metabolism (4.88e-04)
Glycerophospholipid biosynthesis (1.89e-04)
Glycolysis / Gluconeogenesis (8.01e-09)
Core histone genes (2.12e-05)
Metabolism of lipids and lipoproteins (4.51e-06)
Metabolism of vitamins and cofactors (2.72e-04)
The citric acid (TCA) cycle and respiratory electron transport (7.39e-08)
Tryptophan metabolism (2.52e-04)
-1.0
-0.5
0.0
0.5
1.0
log2 Fold Change in Expression
D
Hypothalamus
Binding and Uptake of Ligands by Scavenger Receptors (1.47e-03)
Biosynthesis of unsaturated fatty acids (8.87e-04)
Cholesterol biosynthesis (6.87e-08)
Elastic fibre formation (9.97e-04)
Extracellular matrix organization (7.53e-07)
Fatty Acyl-CoA Biosynthesis (1.09e-03)
Focal adhesion (9.10e-04)
Formation of ATP by chemiosmotic coupling (1.15e-03)
Metabolism of lipids and lipoproteins (1.32e-04)
Post-chaperonin tubulin folding pathway (1.56e-05)
Systemic lupus erythematosus (1.30e-06)
The citric acid (TCA) cycle and respiratory electron transport (3.42e-12)
Viral mRNA Translation (1.33e-10)
0.0
0.5
log2 Fold Change in Expression
E
Liver
ABC transporters (1.03e-03)
Arachidonic acid metabolism (1.16e-07)
Biological oxidations (1.37e-20)
Cholesterol biosynthesis (3.63e-08)
Fatty acid metabolism (1.21e-05)
Fatty Acyl-CoA Biosynthesis (1.01e-03)
Glutathione conjugation (8.81e-05)
Metabolism of lipids and lipoproteins (2.81e-12)
PPAR signaling pathway (6.57e-04)
Starch and sucrose metabolism (4.61e-08)
-1
0
1
log2 Fold Change in Expression

798

Fig 2. Prenatal BPA exposure induced transcriptomic alterations in adipose, hypothalamus and liver. (A) Heatmap of expression changes in adipose, hypothalamus and liver for the top 100 differentially expressed genes (DEGs) affected by BPA. Color indicates fold change of expression, with red and blue indicating upregulation and downregulation by BPA. (B) Venn Diagram demonstrating tissue-specific and shared DEGs between tissues. (C-E) Significantly enriched pathways (FDR < 5%) among DEGs from each tissue. Enrichment p-value (shown in parenthesis following the name of functional annotation) is determined by MSEA. The fold change and statistical significance for the top 5 differentially expressed genes in each pathway are shown. *, $p < 0.05$; **, FDR < 5% in differential expression analysis using DEseq2.

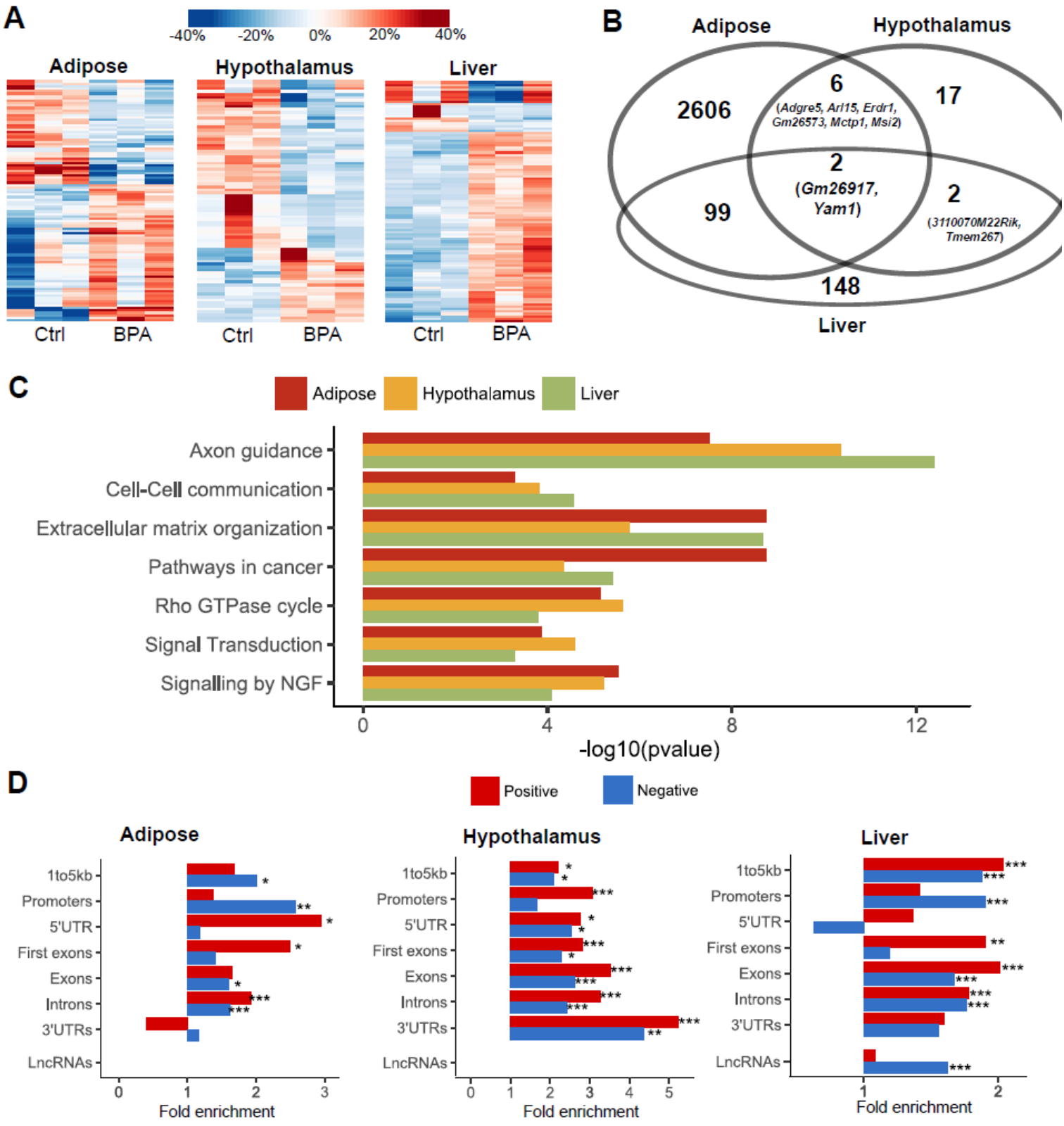
A
-40%
-20%
0%
20%
40%
Adipose
Hypothalamus
Liver
Ctrl
BPA
Ctrl
BPA
Ctrl
BPA
B
Adipose
Hypothalamus
Liver
2606
6
(Adgre5, Arl15, Erdr1, Gm26573, Mctp1, Msi2)
17
2
(Gm26917, Yam1)
99
2
(3110070M22Rik, Tmem267)
148
C
Adipose
Hypothalamus
Liver
Axon guidance
Cell-Cell communication
Extracellular matrix organization
Pathways in cancer
Rho GTPase cycle
Signal Transduction
Signalling by NGF
0
4
8
12
-log10(pvalue)
D
Positive
Negative
Adipose
Hypothalamus
Liver
1to5kb
Promoters
5'UTR
First exons
Exons
Introns
3'UTRs
LncRNAs
Fold enrichment
Fold enrichment
Fold enrichment

807

Fig 3. Prenatal BPA exposure induced methylomic level alteration in adipose, hypothalamus and liver. (A) Heatmap of methylation level changes for the top 100 differentially methylated CpGs (DMCs). Color indicates change in methylation ratio, with red and blue indicating upregulation and downregulation by BPA. (B) Venn Diagram of genes with local DMCs between tissues shows tissue-specific and shared genes mapped to DMCs. (C) Significantly enriched pathways that satisfied FDR < 1% across DMCs from adipose, hypothalamus, and liver tissues. Enrichment p-value is determined by MSEA. (D) Fold enrichment for positive correlations (red bars) or negatively correlations (blue bars) between DMCs and local DEGs, assessed by different gene regions. *, $p < 0.05$; **, $p < 0.01$; ***, $p < 0.0001$; enrichment p-values were determined using Fisher's exact test.

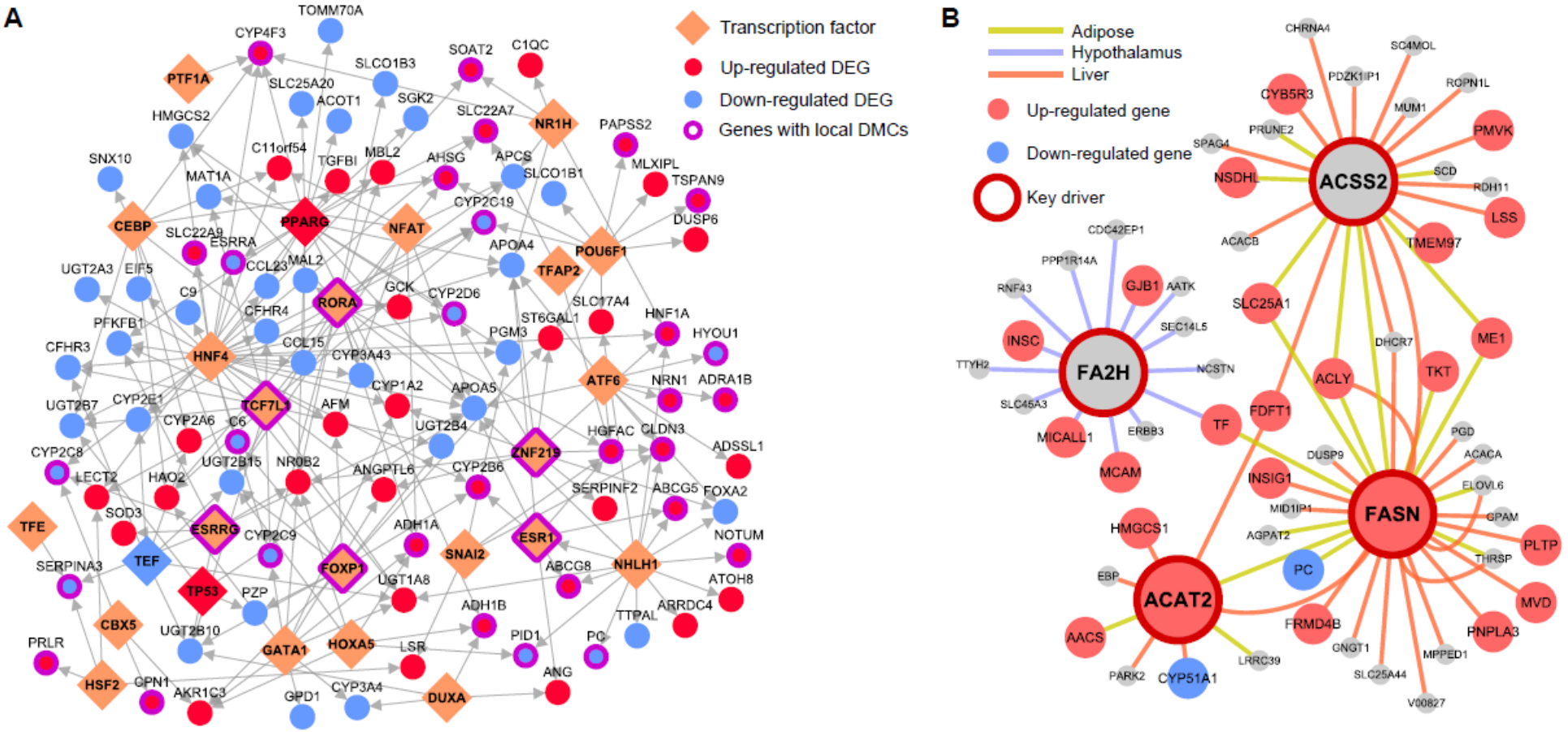

816 **Fig 4. Transcription factors and key drivers orchestrate BPA induced gene expression level changes.** (A) Liver transcription factor
817 regulatory networks for the top ranked transcription factors (FDR < 5%) based on enrichment of liver DEGs among TF downstream targets.
818 Network topology was based on FANTOM5. For TFs with > 20% overlapping downstream targets, only the TF with the lowest FDR is shown. (B)
819 Gene-gene regulatory subnetworks (Bayesian networks) for cross-tissue key drivers. Network topology was based on Bayesian network modeling

of each tissue using genetic and transcriptome datasets from mouse and human populations. For each tissue, if >= 2 datasets were available for a given tissue, a network for each dataset was constructed and a consensus network was derived by keeping only the high confidence network edges between genes (edges appearing in >= 2 studies).

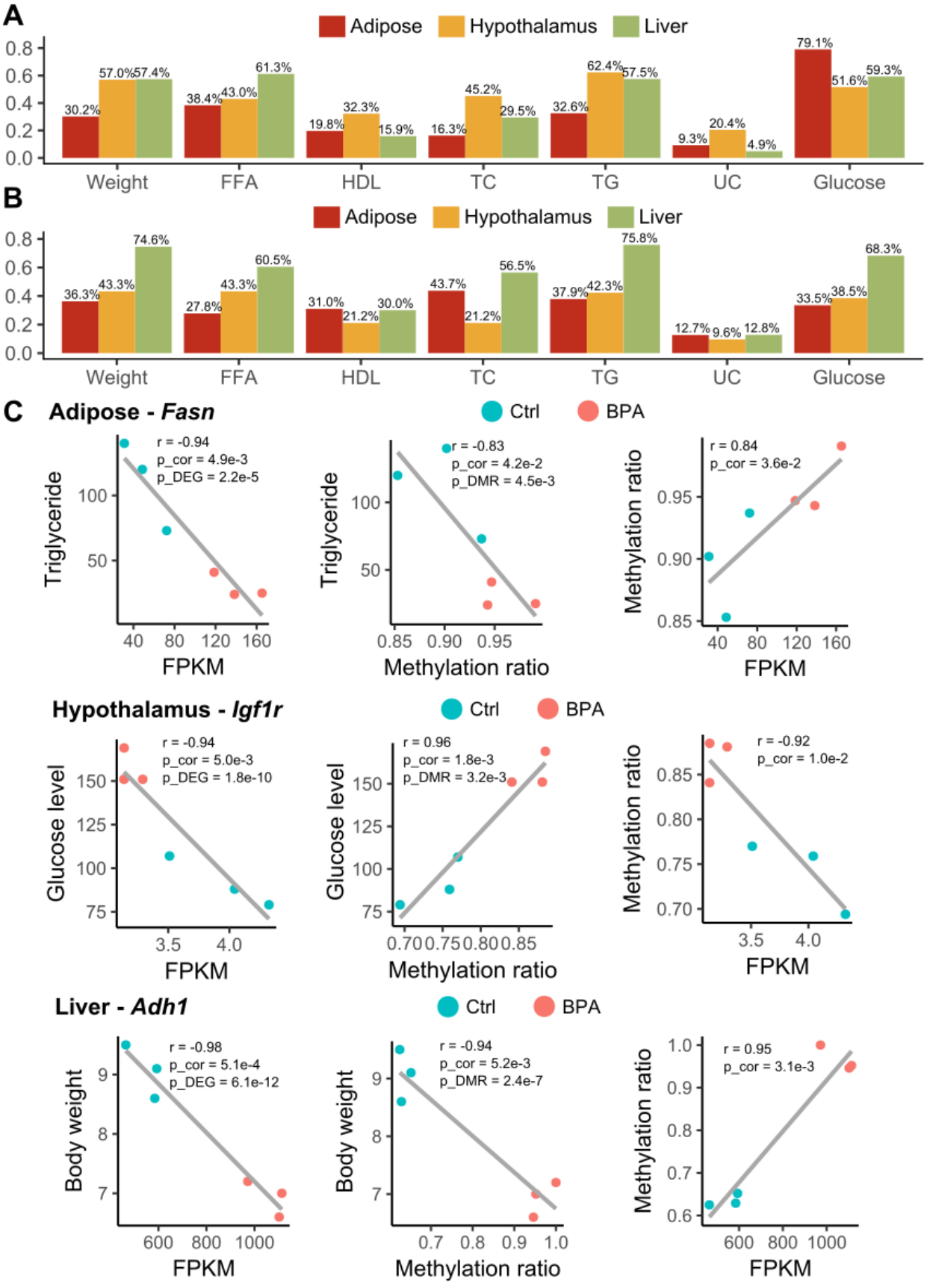
A
Adipose
Hypothalamus
Liver
0.8
0.6
0.4
0.2
0.0
30.2%
57.0%
57.4%
38.4%
43.0%
61.3%
19.8%
32.3%
15.9%
16.3%
45.2%
29.5%
32.6%
62.4%
57.5%
9.3%
20.4%
4.9%
79.1%
51.6%
59.3%
Weight
FFA
HDL
TC
TG
UC
Glucose
B
Adipose
Hypothalamus
Liver
0.8
0.6
0.4
0.2
0.0
36.3%
43.3%
74.6%
27.8%
43.3%
60.5%
31.0%
21.2%
30.0%
43.7%
21.2%
56.5%
37.9%
42.3%
75.8%
12.7%
9.6%
12.8%
33.5%
38.5%
68.3%
Weight
FFA
HDL
TC
TG
UC
Glucose
C
Adipose - Fasn
Ctrl
BPA
r = -0.94
p_cor = 4.9e-3
p_DEG = 2.2e-5
Triglyceride
100
50
40
80
120
160
FPKM
r = -0.83
p_cor = 4.2e-2
p_DMR = 4.5e-3
Triglyceride
100
50
0.85
0.90
0.95
Methylation ratio
r = 0.84
p_cor = 3.6e-2
Methylation ratio
0.95
0.90
0.85
40
80
120
160
FPKM
Hypothalamus - Igf1r
Ctrl
BPA
r = -0.94
p_cor = 5.0e-3
p_DEG = 1.8e-10
Glucose level
150
125
100
75
3.5
4.0
FPKM
r = 0.96
p_cor = 1.8e-3
p_DMR = 3.2e-3
Glucose level
150
125
100
75
0.70
0.75
0.80
0.85
Methylation ratio
r = -0.92
p_cor = 1.0e-2
Methylation ratio
0.85
0.80
0.75
0.70
3.5
4.0
FPKM
Liver - Adh1
Ctrl
BPA
r = -0.98
p_cor = 5.1e-4
p_DEG = 6.1e-12
Body weight
9
8
7
600
800
1000
FPKM
r = -0.94
p_cor = 5.2e-3
p_DMR = 2.4e-7
Body weight
9
8
7
0.7
0.8
0.9
1.0
Methylation ratio
r = 0.95
p_cor = 3.1e-3
Methylation ratio
1.0
0.9
0.8
0.7
0.6
600
800
1000
FPKM

823

Fig 5. Correlation between gene expression, methylation and metabolic traits. (A) Percentage of tissue-specific DEGs that are correlated with metabolic traits ($p < 0.05$). (B) Percentage of tissue-specific DMCs that are correlated with metabolic traits ($p < 0.05$). (A-B) p-values were determined using Pearson correlation test. (C) Pair-wise correlation between expression level, methylation ratio and metabolic profiles (triglyceride, glucose level, body weight) for *Fasn, Igf1r and Adh1*. P_cor, p-value was determined using Pearson correction test; P_DEG was determined using differential expression test; P_DMC was determined using differential methylation test.

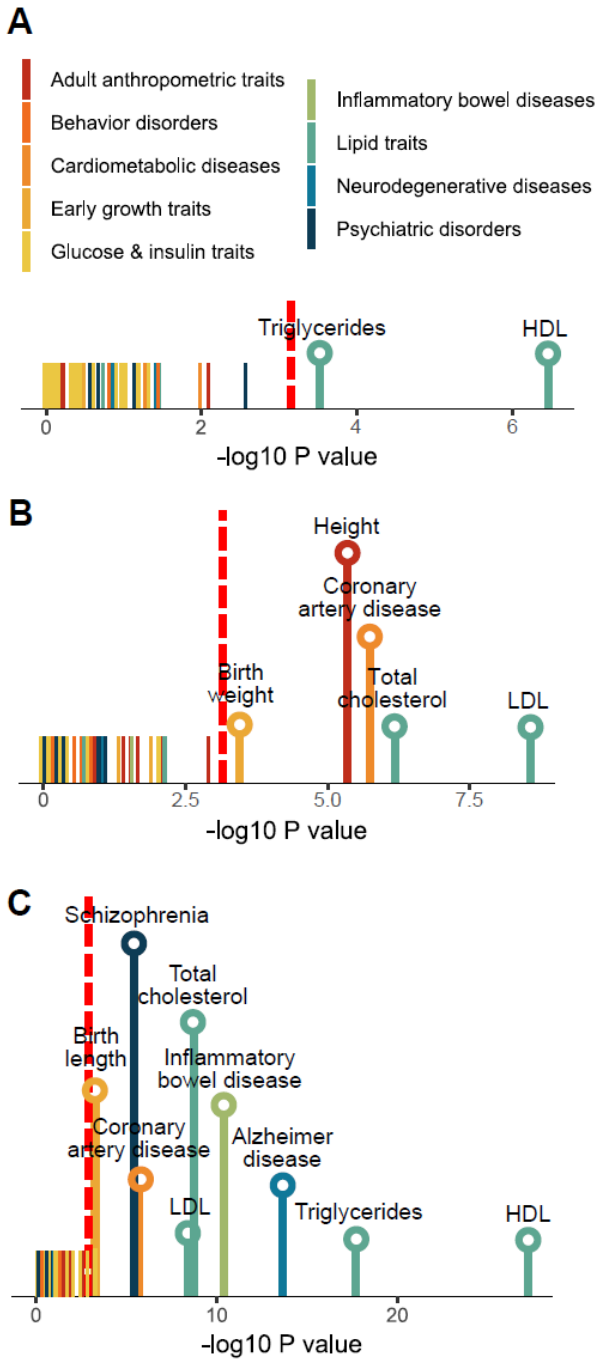

831

832 **Fig 6. Association of differential expression signatures from adipose (A), hypothalamus (B) and liver (C)**

833 **with 61 human traits/diseases, color coded into nine primary categories.** P-values are determined using

834 MSEA. Red dashed line indicates the cutoff for Bonferroni-corrected p = 0.05. Names of traits/diseases whose p-

835 values didn't pass Bonferroni-corrected cutoff were not shown.